Human Activity Classification with Adaptive Thresholding using Radar Micro-Doppler

Zhenghui Li
James Watt School of Engineering
University of Glasgow
Glasgow, United Kingdom
2227284l@student.gla.ac.uk

Francesco Fioranelli
Department of microelectronics
TU Delft
Delft, The Netherlands
f.fioranelli@tudelft.nl

Shufan Yang
School of Computing
Edinburgh Napier University
Edinburgh, United Kingdom
s.yang@napier.ac.uk

Julien Le Kernec
James Watt School of Engineering
University of Glasgow
Glasgow, United Kingdom
Julien.lekernec@glasgow.ac.uk

Qammer Abbasi
James Watt School of Engineering
University of Glasgow
Glasgow, United Kingdom
qammer.abbasi@glasgow.ac.uk

Olivier Romain
ETIS lab
CY university
Cergy-Pontoise, France
olivier.romain@cyu.fr

***Abstract*— Radar systems are increasingly being used for healthcare applications for human activity recognition due to their advantages for privacy compliance, contactless sensing, and insensitivity to lighting conditions. The proposed classification algorithms are often very complex, hence requiring significant computational resources. We propose an adaptive thresholding algorithm used as a 'mask' to highlight the region of interest from the micro-Doppler signature. The mask is then applied to spectrogram information. These masked signatures are used for handcrafted feature extraction and classification. A quadratic-SVM classifier is employed based on the features from the information acquired. The preliminary results show that an accuracy of 91.3% is achieved using sequential forward feature selection with feature fusion. Based on our initial result, a Naïve Bayes combiner is used to improve the overall performance further. With this strategy, the accuracy of classification reaches 92.5% for six activities. Additionally, we compare our findings to those of other models utilizing the same database. The results demonstrate that high accuracy can be achieved when adaptive thresholding is used with the SVM method, and computational resources may significantly decrease.**

Keywords—Human Micro-Doppler, Human activity recognition, Adaptive thresholding, Classification.

I. INTRODUCTION

In recent years, human activity recognition has been required in a series of applications, including healthcare, motion analysis and security surveillance [1-5]. Radar is becoming increasingly irreplaceable in this field due to its unique advantages, compared with wearable devices [6] and image/camera sensors [7], such as insensitivity to lighting and weather condition, privacy compliance (no image of users and private environments are collected), and contactless sensing (no device to wear or carry).

Conventionally, radar-based human activity recognition relies on the Micro-Doppler signature, a powerful representation of body micro-motions, synthesizing the Doppler components induced by different body parts such as limbs, legs, head and fingers [8]. These micro-Doppler signatures contain kinematic characteristics and reflect the exclusive motion pattern of a target, and therefore they are widely used in human activity recognition [9-12]. Du et al. [13] developed a range-velocity-time 3-D model that depicts the motions of different people in a multi-target situation by combining the micro-Doppler signature with range information. In [14], a separation method was proposed to split the individual micro-Doppler components from the multi-target micro-Doppler signatures. The separated components were then trained and tested using a separation convolutional neural network with a residual dense network.

Although the methods with both statistical learning and deep learning in human activity recognition are emerging, most of the current works focus on classification algorithm accuracy instead of computational efficiency and pre-processing of data. This paper proposes an adaptive thresholding method at the pre-processing stage to focus on the region of interest for classification based on [15]. The micro-Doppler signature contains plenty of information from not only the target but the background. This approach is designed to outline the region of interest (ROI) in the spectrogram, the targeted part, also named 'mask'. For the purpose of concurrently increasing accuracy and reducing computational loading, feature selection [16] and information fusion [17] are introduced to further improve overall performance.

The rest of this paper is organized as follows: Section II describes the experimental setup and the methods used in this investigation. Section III presents the result of classification, feature selection and feature fusion, with discussions based on the preliminary results. Section IV draws conclusions and some possible future works.

II. METHODOLOGY

A. Data Collection and Pre-processing

The dataset used in this paper is the University of Glasgow Radar Signature dataset [18, 19]. The data was collected using an off-the-shelf Frequency Modulated Continuous Wave (FMCW) radar, which operates at 5.8 GHz with 400 MHz bandwidth, 1 ms sweep time and 128 complex samples per sweep. A total of 1754 motion files were recorded from 72 participants aged 21 to 98 years old. The dataset was composed of six types of human activities, including walking, sitting down, standing up, picking up an object, drinking water and fall. Note that the dataset is not balanced, i.e. the elderly participants did not perform the 'fall' activity for obvious reasons. This dataset is summarized in Table I.

The raw data are first converted into a range-time map with the steps below. For different types of samples, the duration of recordings varies between 5 and 10 s, where the number of chirps is N = 5000 and N = 10000, respectively. Afterwards, a 128-point Hamming-windowed fast Fourier transform is applied to each chirp, and a 4^{th}-order high-pass

Butterworth notch filter with cut-off frequencies of 0.0075Hz is also used to remove static clutter. After obtaining the range-time map, a Short-Time Fourier transform (STFT) is implemented using a 0.2s Hamming window with 95% overlapping factor on the Range-time map to generate micro-Doppler signatures. Typical micro-Doppler signatures of each type of activity are shown in Fig.1.

TABLE I. SUMMARY OF THE DATASET

No.	Activity Description	Number of samples	Data Length
A1	Walking back and forth	312	10s
A2	Sitting down on a chair	312	5s
A3	Standing up from a chair	311	5s
A4	Picking up an object	311	5s
A5	Drinking water	310	5s
A6	Fall	198	5s

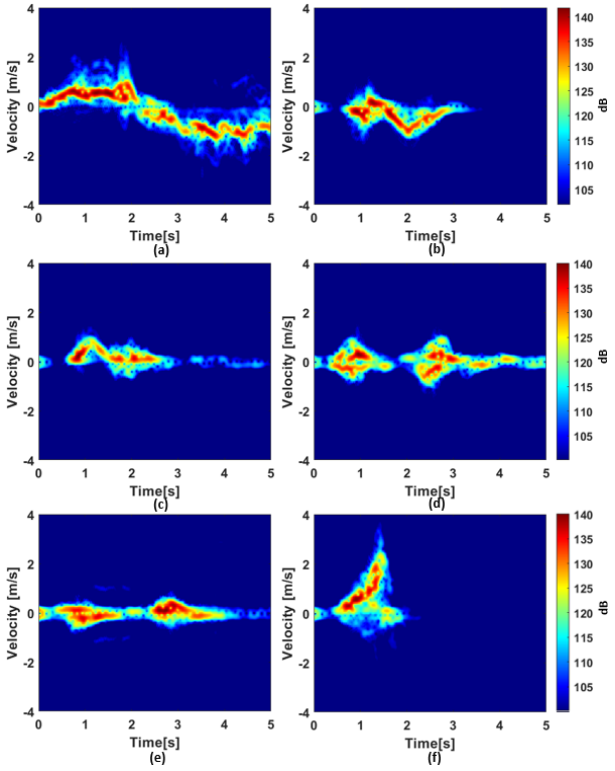

Fig. 1. The micro-Doppler signatures of typical samples. (a)~(f) represent activities A1~A6 micro-Doppler spectrogram.

B. Adaptive Thresholding Methods

The motivation of the proposed adaptive thresholding method is to generate low noise micro-Doppler signature images for further application. As shown in Fig. 1, although the notch filter is implemented, background clutter still occurs in a significant number of pixels. The further feature extraction process would be burdened with these obstructions, which increases the computational complexity and degrades the robustness of the features. Hence, it is critical to define the ROI of the spectrogram.

We can also observe from Fig.1 that the intensity and amplitude of different data are varied, which means it is inappropriate to apply a fixed threshold on all activities. An adaptive thresholding method is introduced to extract the region of interest of each spectrogram.

The proposed method binarizes the grayscale spectrogram image with a specific threshold T. The principle of this method is to select a threshold and then update it based on the information contained in the window being processed to focus on the ROI adaptively. The spectrogram image is firstly converted into a greyscale image. Suppose that the grayscale spectrogram image S has N pixels and each pixel value is represented as $I(x, y)$, the initial threshold μ can be expressed as:

$$\mu = \frac{1}{N} \sum_{I(x,y) \in S} I(x, y) \tag{1}$$

According to the initial threshold value μ, the spectrogram image is divided into two parts: P_1 and P_2, where P_1 is the image region that has a pixel value greater than μ and P_2 is the image region which has a pixel value smaller than μ. Then, a new threshold T can be described as:

$$T = \frac{1}{2}\left[\frac{1}{N_1}\sum_{I(x,y)\in p_1} I(x,y) + \frac{1}{N_2}\sum_{I(x,y)\in p_2} I(x,y)\right] \tag{2}$$

Where N_1 and N_2 denote the number of pixels in part P_1 and P_2, respectively.

After the acquisition of both μ and T, they will be compared with each other. If the difference is greater than 0.1, then T will replace μ to segment the grayscale spectrogram image and calculate a new T through (2). This process is repeated until the difference is smaller than 0.1, which ensures to preserve as much ROI as possible. The final threshold value is implemented to binarize the grayscale spectrogram image. It can be represented as follows:

$$b(x, y) = \begin{cases} 1, & I(x, y) \geq T \\ 0, & I(x, y) < T \end{cases} \tag{3}$$

Where $b(x, y)$ is the pixel value of the mask.

The binarized image can be used for feature extraction as well as a mask on the spectrogram information, subsequently named as mask image and masked spectrogram. The process of acquiring binary mask, and masked spectrogram, are shown in Fig. 2, and they will be utilized for the next processes in this investigation.

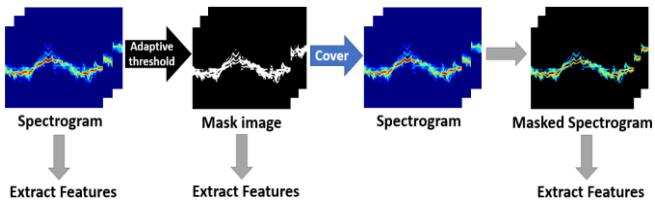

Fig. 2. An example of calculating binary mask to generate mask and masked spectrogram.

C. Feature Processing

Numerous studies, including ours [4, 5], make extensive use of features to portray the data in a more compact and salient manner. In this case, 68 features are extracted from the mask image, of which two categorized are considered: the property of ROI [15] and texture of an image [21]. The first type depicts the geometrical properties of the ROI, such as centroid, perimeter, area, amongst others. The second type is characterized by the spatial distribution of intensity levels within a neighbourhood, which contains information on the spatial arrangements of intensities in an image. All the features calculated in this experiment are listed in Table II. Different features are suggested for the spectrograms in terms of previous literature [18] and our outcomes [5], listed in Table III.

TABLE II. TABLE OF FEATURES FOR MASK IMAGE

ROI Features	Feature Dimensions
Perimeter of ROI	1×1
Area of ROI	1×1
Centroid of ROI	1×2
Eccentricity of ROI	1×1
Orientation of ROI	1×1
Major and Minor Axis Length of ROI	1×2
Textural Features	**Feature Dimensions**
Local Binary Pattern of image	1×59
Moment of image	1×1

TABLE III. TABLE OF FEATURES FOR SPECTROGRAM AND MASKED SPECTROGRAM

RADAR Features	Feature Dimensions
Entropy of spectrogram	1×1
Skewness of spectrogram	1×1
Centroid of spectrogram (mean & variance)	1×2
Bandwidth of spectrogram (mean & variance)	1×2
Energy Curve (mean & variance & Trapezoidal numerical integration)	1×3
Singular Vector Decomposition (mean and variance of the first three vectors of components)	1×12

To further improve the overall performance and reduce the computational complexity, information fusion and feature selection are introduced. The feature selection technique is used to eliminate redundant and duplicate information to increase classification accuracy and decrease computational loading [16]. It can employ three distinct strategies [16]: wrapper methods, filter methods, and embedded methods.

In this case, we evaluate a wrapper method, namely sequential floating forward selection (SFFS). SFFS is based on sequential forward selection (SFS), which determines the optimal feature combinations by ranking the features using a classifier and its accuracy as a measure. Compared with SFS, SFFS not only performs progressive adding but additional removing, which means it eliminates the features from the selected subset when the subset is deemed to be 'better' by the classifier after removal of a particular feature.

Information fusion is an advanced approach that can overcome the limitation of individual domain features by pooling information or decision from different sources. It can be achieved through different levels of abstraction [17], typically divided into signal, feature and decision levels. In this paper, both feature and decision level fusions are used. Feature level fusion cascades the features from different sensors or domains with the same labels, as in Eq. 4, where $\cap$ represents the concatenation of features from different domains.

$$F_{Fusion} = F_{Mask} \cap F_{MaskedSpectrogram} \tag{4}$$

Decision level fusion [17] combines the decisions of several classifiers to produce a single result. Multiple classifiers can be employed with multi-modal sensors and different features. This paper proposes a Naïve-Bayes (NB) combiner [9, 22] to proceed with the decision fusion. The mathematical representation of the NB combiner is shown in Eq. 5.

$$F(S_i) = P(S_i) \bullet \prod_{m=1}^{N} p_{m,k,S_i} \tag{5}$$

$F(S_i)$ indicates the decision factor of class S_i, where S_i is the class of interest. $P(S_i)$ is the support rate of the interest class. For example, there are four classifiers and three of them classify one sample as class S_1, the support rate $P(S_1)$ of this sample is 3/4. $p_{m,S_i,k}$ denotes the (k, S_i) entry in the confusion matrix for the classifier m, whereas the k is the prediction label of the classifier m. The factor is the product of the support rate and the classification confusion matrix entry p (row k, column S_1 and classfier m), and the class of interest with the highest factor will be the final label.

III. RESULTS

We begin by assessing the proposed thresholding technique on spectrograms, and the obtained mask is then used on spectrogram to acquire the masked spectrogram, followed by extracting features and a comparison using conventional classification. Then, feature selection and information fusion are utilized for increasing accuracy.

A. *Thresholding Evaluation*

To investigate the effects of adaptive threshold T, seven thresholds ranging linearly from T-10 to T+20 are applied to spectrograms, and the obtained masks are then applied to the spectrogram. Two distinct categories of data are analysed separately to determine their contribution to classification. At this stage, a robust Quadratic-kernel support vector machine (Q-SVM) algorithm with 10-fold cross-validation is adopted to the activity classification. The results are shown in Table IV and V.

TABLE IV. CLASSIFICATION RESULTS FOR THE MASK IMAGES WITH DIFFERENT THRESHOLDS

%	A1	A2	A3	A4	A5	A6	Avg
T-10	96.8	91.3	87.7	63.0	77.1	89.9	84.3
T-5	97.2	92.1	90.4	63.4	77.6	89.3	85.0
T	97.8	90.7	89.3	62.5	76.7	92.4	84.9
T+5	98.7	93.3	86.9	64.7	69.3	89.9	83.8
T+10	96.1	89.7	90.0	61.2	74.8	90.4	83.7
T+15	97.4	90.4	90.3	64.4	75.1	91.2	84.8
T+20	97.8	91.0	88.4	62.0	74.5	90.4	84.0
Avg	97.4	91.2	89.0	63.0	75.1	90.5	

TABLE V. CLASSIFICATION RESULTS FOR THE MASKED (WITH DIFFERENT THRESHOLDS) OR UNMASKED SPECTROGRAM

%	A1	A2	A3	A4	A5	A6	Avg
No Mask	94.0	80.2	82.4	63.6	73.7	87.9	80.3
T-10	100	87.1	86.3	61.2	70.8	93.1	83.1
T-5	100	89.3	87.9	62.6	72.1	92.4	84.1
T	100	91.3	89.2	63.9	75.5	94.4	85.7
T+5	100	89.6	88.4	62.1	71.8	94.4	84.4
T+10	100	88.0	87.7	61.5	70.3	93.9	83.6
T+15	99.7	87.1	86.3	63.0	69.6	92.4	83.0
T+20	99.7	86.7	85.6	64.4	67.9	91.7	82.6
Avg	99.9	88.4	87.3	61.7	71.1	93.2	

From the above tables, it can be seen that the highest average accuracy of 85.7% is achieved when the masked spectrogram is used with threshold T without offset. Also, 85% of accuracy has been attained using mask images. Note that the binary mask allows a 10-fold reduction in memory requirements to hold the input database, given the limited

resources on an embedded platform, which is a significant step. Generally, the features extracted from the masked spectrogram have the best overall performance. The masked spectrogram obtained its best overall result with threshold T without offset, and the mask image achieves its highest accuracy when the threshold is T-5, which means the exploration in the range of thresholding has positive effects on the results. The spectrogram without mask generally has 3.5% performance degradation compared with mask image and masked spectrogram. It is mainly because the accuracy decreases greatly in A2, approximately 11.2% and 8.2%, respectively. A1, A3 and A6 also decrease slightly in accuracy, with ~4.5%, 5.5% and 4% for both domains, respectively. Also note that different thresholds yield the best accuracy per activity. For instance, 64.4% accuracy is achieved for picking an object with T+20 in the masked spectrogram domain.

B. *Feature Level Fusion and Feature Selection*

After analysing the performances of the mask image, spectrogram, and masked spectrogram individually, they are combined with feature level fusion. Based on the previous results, in the feature level fusion part, we only choose the features extracted from mask images with threshold T-5 and masked spectrogram with threshold T because they have the best overall performance in their domains. At this stage, the Q-SVM and 10-fold cross-validation are still used. The results are shown in Table VI. Generally, the fusion of two types of data yields the best result, with an accuracy of 90.2%. Compared with individually using different domains of data, the fusion has an improvement in accuracy, increased by 5.2% for the mask, 4.5% for the masked spectrogram.

TABLE VI. CONFUSION MATRIX OF FEATURE LEVEL FUSION RESULTS

%		Predicted Label					
		A1	A2	A3	A4	A5	A6
True Label	A1	100	0	0	0	0	0
	A2	0	95.4	0	2.3	2.3	0
	A3	0	0	96.1	2.6	0.9	0.4
	A4	0	1.0	1.9	79.4	17.2	0.5
	A5	0	1.1	0	23.1	75.8	0
	A6	0	0	4.1	1.4	0	94.5

To further explore the influence caused by feature type and feature domain, as well as reduce the computational loading and evaluate the feature selection approach, the SFFS algorithm is applied to the individual results with the highest accuracy for both mask and masked spectrogram. The feature level fusion result and the original spectrogram are also considered to investigate the effectiveness of our thresholding methods and fusion methods. The results are shown in Fig. 3 and Table VII.

TABLE VII. COMPARISON USING FEATURE SELECTION

Methods	No. of Original Features	No. of Selected Features	Accuracy (%)
Mask image	68	16	86.9
Spectrogram	21	12	84.7
Masked spectrogram	21	13	87.4
Fusion of mask images and masked spectrogram	89	30	91.3

Although the SFFS provides limited improvements in accuracy, it significantly reduces the number of features. Generally, the number of features is reduced to one-third of the starting count. The accuracy generally increases by approximately 2% for individually used data and by 1.1% for fusion results. Note that the masked spectrogram provides the most lightweight implementation with the highest accuracy for individual data domains with 13 features and 87.4%. For the fusion data, 91.3% accuracy is obtained with 30 features out of the original 89, which is even fewer features than the mask domain before feature selection (68 features).

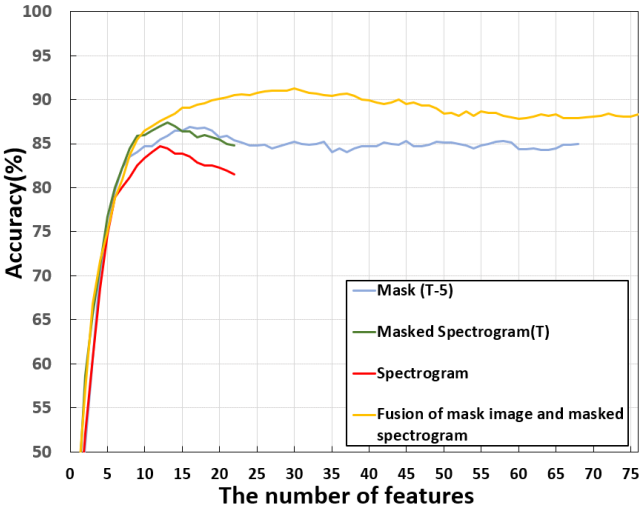

Fig. 3. Feature selection with SFFS for individuals and fusion approaches

C. *Decision Level Fusion*

Based on the previous results, the decision level fusion approach is applied for optimising classification. Four classifiers, including mask images with threshold T-5, spectrogram, masked spectrogram with threshold T and feature level fusion, are combined with NB combiner. The result is shown in Fig. 4.

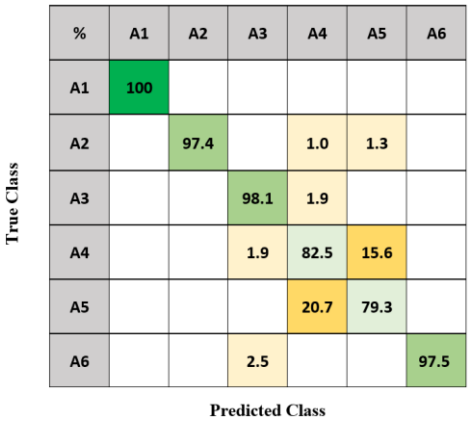

Fig. 4. Confusion matrix of Naïve Bayes Combiner with four classifiers.

The NB combiner has an average accuracy of 92.5%, which improved by 1.2% compared with the highest accuracy using feature level fusion. The NB combiner outperforms every type of activity. A4 and A5 have the greatest improvements, which are over 3%. The other four activities also improve approximately 2% to 3%. We also compare our results with different models using the same database [20]. They are listed in Table VIII. This paper uses adaptive thresholding with the SVM algorithm, which can not only achieve high accuracy but also greatly reduced the use of

resources. This is also beneficial for further convenience to migrate to embedded devices.

TABLE VIII. COMPARISON USING FEATURE SELECTION

Model	Accuracy
VGG 19	56%
Resnet50	91.1%
Mnasnet	90.1%
Densenet101	90.5%
Shufflenet	90.1%
Adaptive threshold – feature level fusion with SFFS	91.3%
Adaptive threshold fusion with NBC	**92.5%**

IV. CONCLUSION

In this paper, we investigate the feasibility of an adaptive thresholding method in human activity recognition using radar. Features are extracted from two data domains (mask image, masked or unmasked spectrogram) and trained with a Q-SVM classifier. The feature level fusion and SFFS selection approach is then used with threshold T-5 for mask and threshold T for masked spectrogram that offered the best average accuracy of 91.3%. Based on our preliminary results, we also propose a decision level fusion approach using NB combiner that achieves 92.5% accuracy. We have shown that a lightweight implementation of statistical learning combined with efficient pre-processing can outperform deep learning techniques and bring us one step closer to the implementation on resource-constrained embedded platforms.

In future work, the range of thresholds could be expanded for more exploration. Different classifiers, feature selection approaches, and even other types of classification, such as hierarchical structure [5], might be investigated. Also, the exploration of evolutionary genetic algorithms can be used to further optimise the general performances of classification [23].

ACKNOWLEDGMENT

The authors would like to thank the British Council 515095884 and Campus France 44764WK—PHC Alliance France-UK, and PHC Cai Yuanpei – 41457UK for their financial support. .

REFERENCES

[1] H. Li, A. Shrestha, H. Heidari, J. L. Kernec and F. Fioranelli, "Activities Recognition and Fall Detection in Continuous Data Streams Using Radar Sensor," 2019 IEEE MTT-S International Microwave Biomedical Conference (IMBioC), 2019, pp. 1-4.

[2] S. Hazra and A. Santra, "Robust Gesture Recognition Using Millimetric-Wave Radar System," in IEEE Sensors Letters, vol. 2, no. 4, pp. 1-4, Dec. 2018.

[3] J. Le Kernec et al., "Radar Signal Processing for Sensing in Assisted Living: The Challenges Associated With Real-Time Implementation of Emerging Algorithms," IEEE Signal Processing Magazine, vol. 36, no. 4, pp. 29-41, 2019.

[4] Z. Li, J. Le Kernec, F. Fioranelli, O. Romain, L. Zhang and S. Yang, "An LSTM Approach to Short-range personnel recognition using Radar Signals," 2021 IEEE Radar Conference (RadarConf21), 2021, pp. 1-6, doi: 10.1109/RadarConf2147009.2021.9455218.

[5] X. Li, Z. Li, F. Fioranelli, S. Yang, O. Romain, and J. L. Kernec, "Hierarchical Radar Data Analysis for Activity and Personnel Recognition," Remote Sensing, vol. 12, no. 14, p. 2237, Jul. 2020.

[6] T. R. Bennett, J. Wu, N. Kehtarnavaz, and R. Jafari, "Inertial measurement unit-based wearable computers for assisted living applications: A signal processing perspective," IEEE Signal Process. Mag., vol. 33, no. 2, pp. 28–35, 2016.

[7] D. T. Nguyen, H. G. Hong, K. W. Kim, K. R. Park, "Person Recognition System Based on a Combination of Body Images from Visible Light and Thermal Cameras," Sensors, vol. 17, pp. 605, 2017.

[8] Y. Kim and H. Ling, "Human activity classification based on micro doppler signatures using a support vector machine," IEEE Transactions on Geoscience and Remote Sensing, vol. 47, no. 5, pp. 1328–1337, 2009.

[9] H. Li, J. Le Kernec, A. Mehul, S. Z. Gurbuz and F. Fioranelli, "Distributed Radar Information Fusion for Gait Recognition and Fall Detection," 2020 IEEE Radar Conference (RadarConf20), 2020, pp. 1-6.

[10] S. Z. Gurbuz and M. G. Amin, "Radar-Based Human-Motion Recognition With Deep Learning: Promising Applications for Indoor Monitoring," in IEEE Signal Processing Magazine, vol. 36, no. 4, pp. 16-28, July 2019.

[11] B. Jokanović and M. Amin, "Fall Detection Using Deep Learning in Range-Doppler Radars," in IEEE Transactions on Aerospace and Electronic Systems, vol. 54, no. 1, pp. 180-189, Feb. 2018.

[12] M. S. Seyfioğlu, A. M. Özbayoğlu and S. Z. Gürbüz, "Deep convolutional autoencoder for radar-based classification of similar aided and unaided human activities," in IEEE Transactions on Aerospace and Electronic Systems, vol. 54, no. 4, pp. 1709-1723, Aug. 2018.

[13] H. Du, T. Jin, M. Li, Y. Song and Y. Dai, "Detection of multi-people micro-motions based on range–velocity–time points," in Electronics Letters, vol. 55, no. 23, pp. 1247-1249, 2019.

[14] X. Huang, J. Ding, D. Liang and L. Wen, "Multi-Person Recognition Using Separated Micro-Doppler Signatures," in IEEE Sensors Journal, vol. 20, no. 12, pp. 6605-6611, June. 2020.

[15] O. Romain, J. Le Kernec, J. Lorandel, and F. Fioranelli, "Dispositif de caracterisation de l'actimetrie d'un sujet en temps reel," Device for Characterizing the Actimetry of a Subject in Real Time", WO2021069518A1, Oct 2019.

[16] I. Guyon and A. Elisseeff, "An introduction to variable and feature selection," The Journal of Machine Learning Research, vol. 3, pp. 1157–1182, 2003.

[17] R. C. Luo, Chih-Chen Yih and Kuo Lan Su, "Multisensor fusion and integration: approaches, applications, and future research directions," in IEEE Sensors Journal, vol. 2, no. 2, pp. 107-119, April 2002.

[18] F. Fioranelli, S.A. Shah, H. Li, A. Shrestha, S. Yang, J. Le Kernec, "Radar sensing for healthcare," IET Electronic Letters, 55(19), pp. 1022-1024, 2019.

[19] F. Fioranelli, S. A. Shah, H. Li, A. Shrestha, S. Yang, J. Le. Kernec, "Radar signatures of human activities," URL: http://researchdata.gla.ac.uk/id/eprint/848, University of Glasgow, 2019.

[20] X. Zhou, T. Jin, and H. Du, "A lightweight network model for human activity classifiction based on pre-trained mobilenetv2," 2020 IET international radar conference, 2021, pp. 1483-1487.

[21] M. S. Karis, N. R. A. Razif, N. M. Ali, M. A. Rosli, M. S. M. Aras and M. M. Ghazaly, "Local Binary Pattern (LBP) with application to variant object detection: A survey and method," 2016 IEEE 12th International Colloquium on Signal Processing & Its Applications (CSPA), 2016, pp. 221-226.

[22] L. Kuncheva and J. Rodríguez, "A weighted voting framework for classifiers ensembles", Knowledge and Information Systems, vol. 38, 2014.

[23] W. Deng, S. Shang, X. Cai, et al., "An improved differential evolution algorithm and its application in optimization problem," Soft Computing, vol. 25, pp. 5277–5298, 2021.